NANO LETTERS

pubs.acs.org/NanoLett

Letter

Porosity Development at Li-Rich Layered Cathodes in All-Solid-State Battery during *In Situ* Delithiation

Shuang Li, Yipeng Sun, Ning Li, Wei Tong, Xueliang Sun, Charles T. Black, and Sooyeon Hwang*

Cite This: *Nano Lett.* 2022, 22, 4905−4911

Read Online

ACCESS | Metrics & More | Article Recommendations | Supporting Information

ABSTRACT: Structural evolutions are crucial for determining the performance of high-voltage lithium, manganese-rich layered cathodes. Moreover, interface between electrode and electrolyte plays a critical role in governing ionic transfer in all-solid-state batteries. Here, we unveil two different types of porous structure in $Li_{1.2}Ni_{0.2}Mn_{0.6}O_2$ cathode with LiPON solid-state electrolyte. Nanopores are found near the cathode/electrolyte interface at pristine state, where cation mixing, phase transformation, oxygen loss, and Mn reduction are also found. *In situ* Li^+ extraction induces the evolution of nanovoids, initially formed near the interface then propagated into the bulk. Despite the development of nanovoids, layered structure is conserved, suggesting the nature of nanopores and nanovoids are different and their impact would be divergent. This work demonstrates the intrinsic interfacial layer, as well as the dynamic scenario of nanovoid formation inside high-capacity layered cathode, which helps to understand the performance fading in cathodes and offers insight into the all-solid-state battery design.

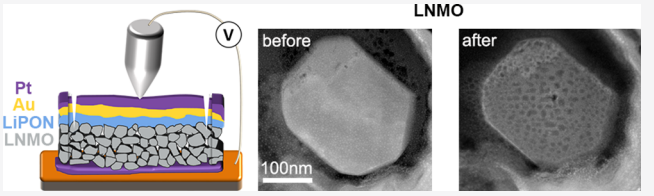

KEYWORDS: *Lithium-ion battery, in situ TEM, all-solid-state battery, layered cathode, nanovoid*

Rechargeable lithium-ion batteries (LIBs) have been successfully commercialized for more than two decades but still have bottlenecks for expanding their applications to emerging markets, such as electric vehicles and transportation systems. One of the major constraints is insufficient energy density intrinsically limited by the deliverable capacities of electrode materials, especially the cathode side.[1−3] Among the reported cathode materials so far, layered lithium- and manganese-rich oxides (LMROs) have exhibited promising performances such as high capacities (up to above 300 $mAhg^{-1}$) and superb cost effectiveness.[4,5] While conventional stoichiometric lithium transition metal oxides ($LiTMO_2$ where TM is transition metal) operate solely based on TM redox, the additional oxygen redox activity in LMROs helps to achieve higher reversible capacity at high-voltage cycling.[6−9] The other limitation of LIBs is safety concerns as liquid electrolytes inside are combustible. All-solid-state LIBs (ASSLB) have received tremendous attention from both academia and industry in recent years as they hold the potential to circumvent the safety issues by replacing flammable organic liquid electrolytes. Furthermore, ASSLBs possibly deliver higher energy density by enabling the use of lithium metal as the anode.[10,11] Among the solid electrolytes, lithium phosphorus oxynitride (LiPON) shows reasonable compatibility with both Li metal anode and cathode,[12−14] demonstrating excellent performance for LiPON-based ASSLB.[15]

Physical and chemical properties of interface between the electrode and electrolyte have been considered as prime factors to determine the electrochemical properties of electrodes. For example, performance degradation of LMRO, such as large irreversible capacity loss in the first cycle, poor rate capability, and severe voltage decay under high charged voltages, is attributed to the aggravating cathode−electrolyte interfacial reactions, which typically leads to the formation of a Li-ion-blocking cathode electrolyte interphase layer,[16,17] surface structural reconstruction,[18−20] consumption of liquid electrolyte,[21] surface corrosion and TM dissolution.[22] The oxygen vacancies formed at the surface and migrated toward the inside lattice are also found to be responsible for the bulk degradation.[23] Compared to the widely studied interfacial reactions with liquid electrolyte as mentioned above, the understanding in the interfacial reactions with solid electrolyte is insufficient even though it is generally accepted that characters of interface between electrode and electrolyte play an important role in governing overall performances of ASSLB.[24,25] A previous investigation reported the formation of disordered $LiCoO_2$ between $LiCoO_2$ cathode and LiPON electrolyte,[26] but a detailed microstructure had not been identified. Atomic arrangement is of particular importance for cathode materials with layered structure because their well-defined atomic structure facilitates two-dimensional lithium diffusion. Therefore, thorough exploration of phase change

Received: April 7, 2022
Revised: June 6, 2022
Published: June 10, 2022

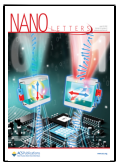

https://doi.org/10.1021/acs.nanolett.2c01401
Nano Lett. 2022, 22, 4905−4911

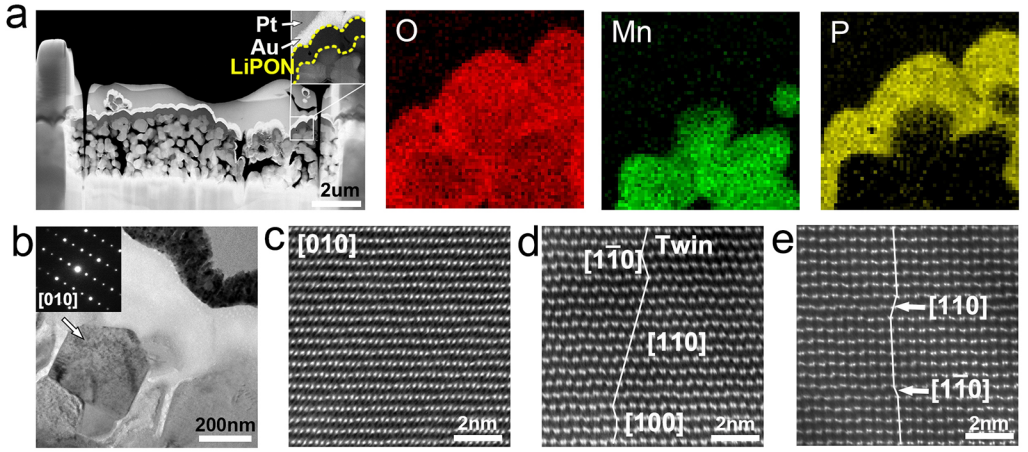

Figure 1. (a) Low-magnification HAADF-STEM image of the all-solid-state LIB sample for *in situ* experiment and the corresponding EELS element mapping of the inset area. (b) The BF-TEM image of the interface between LiPON solid electrolyte and LNMO cathode. The insert is the SAED pattern of the LNMO particle. (c−e) Atomic scale HAADF-STEM images of the LNMO cathode along the [010], [110], and [100] zone axis with small domains.

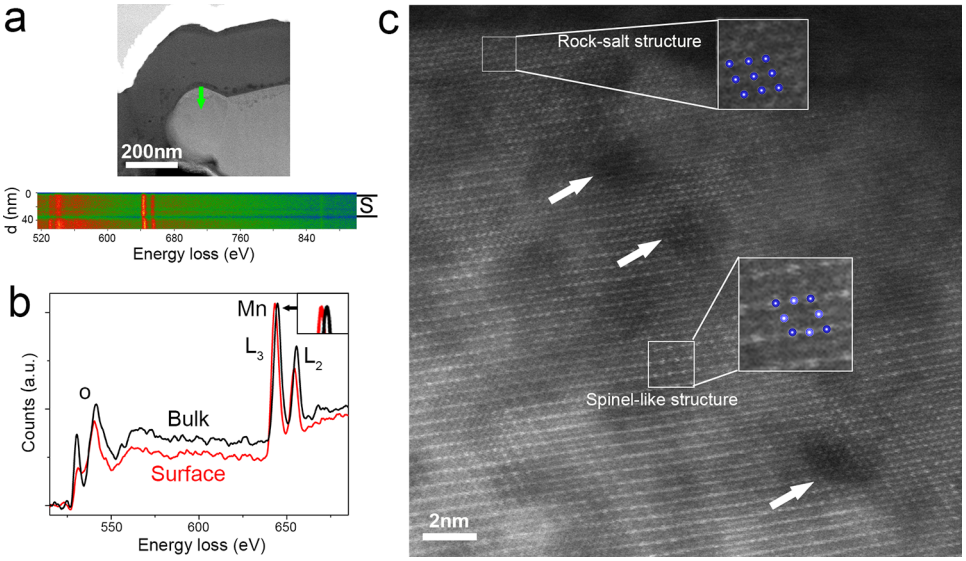

Figure 2. (a) HAADF-STEM image and the corresponding EELS line scan spectra along the green arrow. The S denotes the surface layer of LNMO particle. (b) The EELS O K-edge and Mn L-edge from the surface and bulk region in (a). (c) Atomic scale HAADF-STEM images of the surface region of LNMO cathode along the [010] zone axis. The white arrows indicate areas having nanopores.

induced by interfacial reaction is essential to understand the functioning mechanism of ASSLB. Besides the atomic arrangement at the interface, structural evolutions of the cathode material itself undoubtedly impact the electrochemical performances. Monitoring the structural changes under operation in real time paves a way toward a thorough understanding of structure-process-property relationship. The open-cell setup inside the TEM chamber is an excellent method to study the dynamic structural changes occurring at the cathode in ASSLB under electrochemical processes.[27−31]

Here, we investigate the surface of $Li_{1.2}Ni_{0.2}Mn_{0.6}O_2$ (LNMO) cathode facing the LiPON electrolyte, as well as dynamic microstructural evolutions in LNMO upon delithiation by *in situ* biasing on a cross-sectional solid-state cell. We find an inherent surface reaction between LNMO and LiPON, featuring the formation of surface reconstruction layer with oxygen loss, Mn reduction, phase transformation, and the formation of nanopores. While applying voltage, nanovoids start appearing initially near the interface with LiPON by the Li^+ extraction. Further lithium removal promotes the growth of nanovoids toward the inside of the LNMO particle. It is noteworthy that there is no obvious phase transformation near the biasing-induced nanovoids in the bulk, which is different from the inherent nanopores in surface region adjoined to the electrolyte. Our results demonstrate the LiPON solid electrolyte-induced surface reconstruction layer and dynamic scenario of biasing-induced nanovoid formation during delithiation, which help unveil the origin of performance fading in Li- and Mn-rich layered cathode inside ASSLB.

The LNMO primary particles were pressed to form a pellet, then 250 nm of LiPON solid electrolyte was deposited on the surface of a cathode electrode by RF-magnetron sputtering. The cross-section TEM specimen was prepared by focused ion beam (FIB) to characterize pristine LNMO and the interface between LNMO and LiPON. The Au and Pt layers were deposited on the surface of LiPON to protect the materials of

https://doi.org/10.1021/acs.nanolett.2c01401
Nano Lett. 2022, 22, 4905−4911

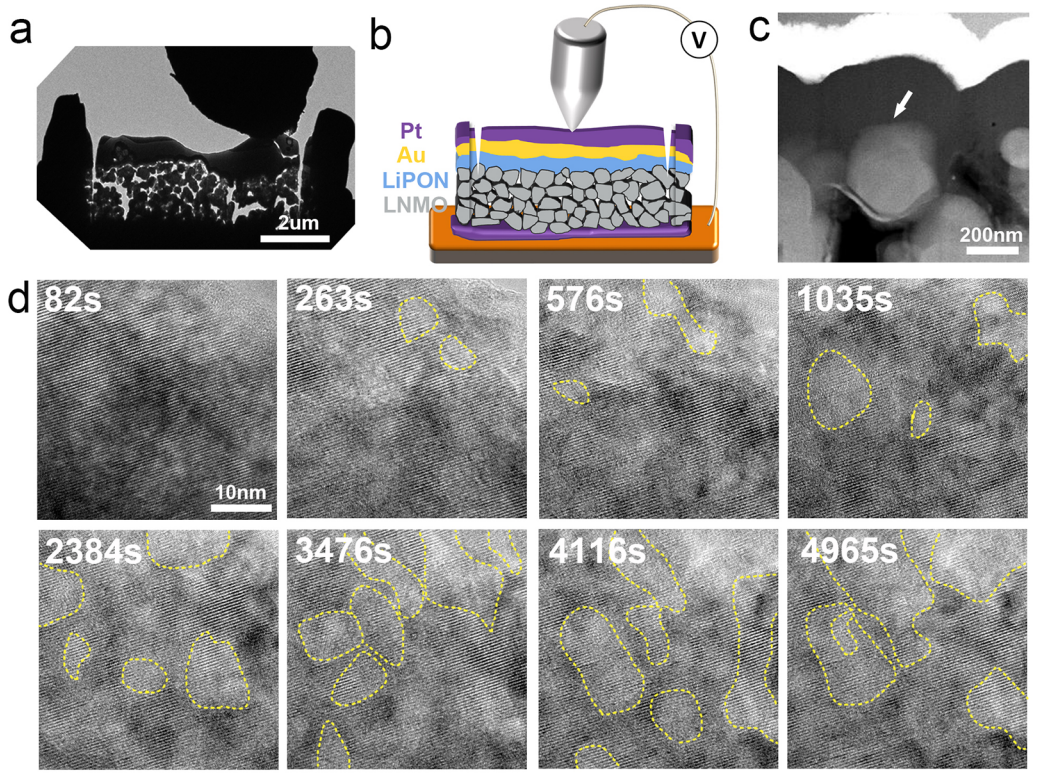

Figure 3. (a,b) Low-magnification TEM image and schematic of the *in situ* experimental setup. (c) The HAADF-STEM image of the observed particle near the cathode/electrolyte interface. (d) Time-lapsed HRTEM images of the LNMO particle obtained from the region near the surface (marked by white arrow in (c)), showing the delithiation-induced nanovoid formation. The yellow dash lines indicate the nanovoids.

interest during the ion milling. Metal layers also served as the top electrode for the subsequent *in situ* biasing, which were cut out from two sides to avoid a possible short circuit. The detailed FIB milling process is described in Experimental Details section in Supporting Information.

Figure 1a shows a low-magnification high-angle annular dark-field scanning TEM (HAADF-STEM) image of the whole specimen and corresponding elemental distributions obtained with electron energy loss spectroscopy (EELS). The Pt, Au, and LiPON layers can be easily distinguished by Z-contrasts in the HAADF-STEM, which has positive correlation with atomic number as indicated in the inset. The Mn and P elemental maps represent the LNMO particles and LiPON layer, respectively, which confirm the successful deposition of LiPON on LNMO. Figure 1b presents a bright-field TEM image of the interface between electrolyte and cathode, showing the well-preserved interface without physical damages from the specimen preparation. The inset of Figure 1b, a selected area electron diffraction (SAED) pattern from the LNMO particle, indicates LNMO particle is well crystallized with a layered monoclinic structure (space group of $C2/m$). The atomic-resolution HAADF-STEM images in Figure 1c−e also demonstrate the layered monoclinic structure with evident Li ordering in the TM layer. Figure 1c shows the [010] zone axis projection with well-arranged layered structure. Atomic arrangement with defects is also found: LNMO in Figure 1d is mainly oriented along [110] but small domains oriented along [100] and $[1\bar{1}0]$ also exist, and Figure 1e exhibits the [100] axis projection dominating with small domains oriented along [110] and $[1\bar{1}0]$. Similar microstructure with multiple orientations (also called variants of monoclinic structures) have been reported in previous studies.[19,32−35] The presence of small domains with different orientations implies the high density of stacking fault.

Because the interface between electrode and electrolyte is important in governing the transport of lithium ions, we first diagnose the structure and chemistry at the interface. Figure 2a displays a HAADF-STEM image and an intensity profile from an EELS line scan acquired from the interface to the interior of LNMO. The obvious differences in oxygen *K*-edge and Mn *L*-edge are observed at the surface of LNMO facing with LiPON, marked by *S* compared to the bulk LNMO. To explore the changes in the chemistry of the surface layer in detail, the EELS spectra (Figure 2b) are extracted both at the surface (from the interface to 40 nm toward inside of particle) and at bulk particle. According to the previous theoretical calculations and experimental results,[26,36,37] the O *K*-pre-edge located at ∼530 eV is attributed to hybridized bonding between TM-3d and oxygen-2p orbitals. The significantly decreased intensity of O *K*-pre-edge in the surface layer thereby could be induced by various reasons, such as formation of oxygen vacancies,[21,23] TM migration accompanied by structural changes,[18] and reduction of TM.[21,38] The reduction of TM in the surface layer is also confirmed by the Mn $L_{2,3}$-edge, which features a chemical shift to lower energy loss and a higher L_3/L_2 intensity ratio. The formation of oxygen vacancies is expected based on the charge neutrality, which also contributes to the lower intensity of O *K*-pre-edge.[39] In addition to the chemical evolution, noticeable structural changes are found at the surface of LNMO in contact with LiPON, such as spinel-like and rock-salt structures and nanopores with a size of ∼2 nm (areas having darker contrast in Figure 2c). Those indicate the significant chemical and microstructural modifications occur at the surface of LNMO. The changes in the surface layer are

https://doi.org/10.1021/acs.nanolett.2c01401
Nano Lett. 2022, 22, 4905−4911

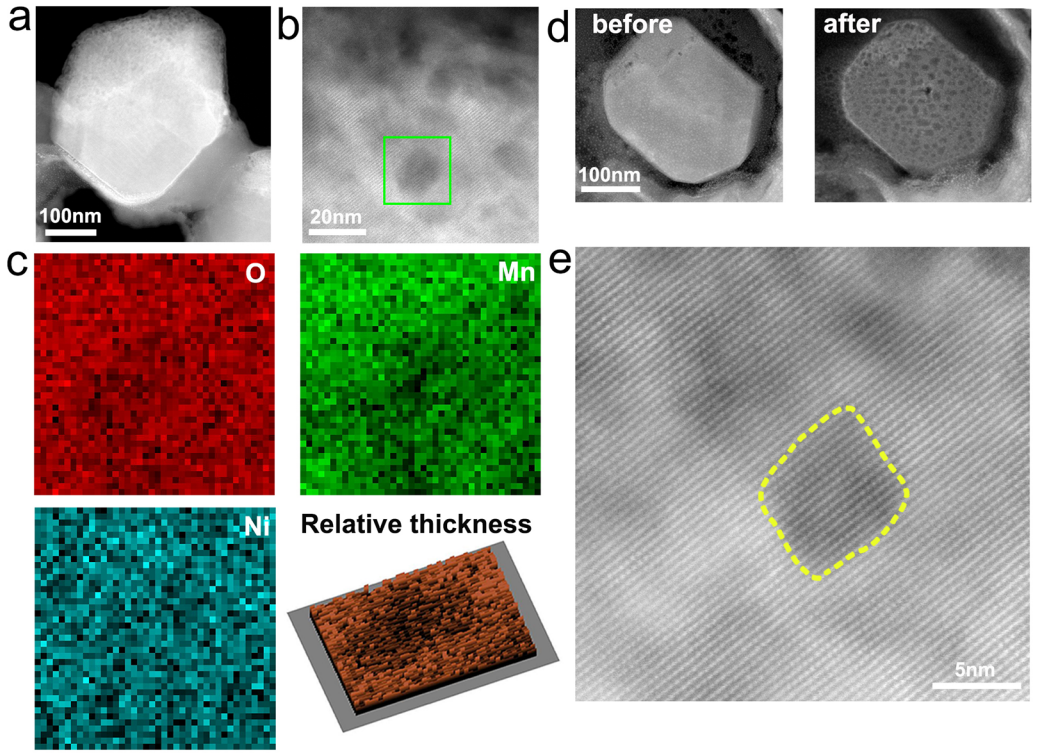

Figure 4. (a,b) The HAADF-STEM images of the observed LNMO particle in Figure 3 after delithiation. (c) The corresponding EELS element and the 2D relative thickness mapping of the void region marked by a green rectangle. (d) The HAADF-STEM images of other LNMO particle before and after delithiation. (e) Atomic scale HAADF-STEM images of the nanovoid region in (b). The yellow dashed line indicates the nanovoid.

suspected to come from the inherent chemical instability between LiPON and LNMO because the nanopores and phase-transformed cubic phases only exist at the surface of LNMO adjacent to the LiPON electrolyte as shown in Figure S1a. It is noteworthy that the uniform layered structure is seen at LNMO particles far from the electrolyte (Figure S1b,c). Chemical instability of LiPON with a $LiCoO_2$ was also reported with the formation of disordered $LiCoO_2$ at the interface,[26,40] which is in line with our observation.

The electrochemical open cell was built based on a nanofactory biasing sample holder inside TEM chamber to track the charge (delithiation) reaction in real time as shown in Figure 3a,b. The tungsten tip was contacted to the top electrode layers (Pt/Au) with a negative bias to extract lithium ions out of the LNMO cathode. Despite the disordered nature of the surface of LNMO, lithium ionic conduction is still successful with percolating channels.[41] The monitored current shows positive correlation with the biasing voltage (Figure S2a) and decreases gradually during the delithiation (Figure S2b), which also substantiate the occurrence of lithium extraction. However, it is not straightforward to correlate the current with the state of charge of the cathode because we cannot correctly estimate the weight of the FIB sample; ionic and electronic transport may be hampered by porous cathode structure, and there might be side reactions at the material deposited during FIB process. For real time observation, we chose a particle in contact with LiPON, where the charge reaction is supposed to start immediately (Figure 3c). The video recorded during *in situ* delithiation at LNMO particle is available in SI Video 1 and corresponding time-lapsed HRTEM images are presented at Figure 3d and Figure S3. Electron dose was kept ~30 pA/cm^2 during observation. Initially, the area of interest looks well crystallized with uniform thickness (82 s of biasing). Interfacial reaction-induced nanopores may exist here, but they are barely recognized as the contrast from tiny pores in an HRTEM image is not as straightforward as that in a HAADF-STEM image (Figure S4). At 263 s, the voids start to appear near the surface or the area close to the electrolyte. The emergence of nanovoids was determined by the changes in image contrasts in SI Video 1. It is noteworthy that biasing-induced nanovoids are much bigger than the inherent nanopores at the interface with LiPON. We define nanopores as the holes formed by the interfacial reaction with LiPON while nanovoids are the empty spaces induced by *in situ* biasing in this work. Further biasing (or delithiation) promotes the growth of each nanovoid and the coalescence of several voids (at 576 s). As more lithium ions are being extracted, the nanovoids gradually propagate toward the bulk with increasing size and volume ratio (Figure S5). We additionally performed a control experiment to see whether the electron beam affects the evolution of the nanovoids. Another video (SI Video 2 and time lapsed images in Figure S6) was obtained under the same electron dose at which SI Video 1 was acquired but without applying bias. The image becomes a little hazy after long-time exposure because of possible carbon contamination, but no nanovoid is found in the viewing region. In other words, electron beam is not responsible for the formation of nanovoids but the lithium extraction is.

Figure 4a–c exhibits the HAADF-STEM images and EELS analyses of the particle in Figure 3 after *in situ* delithiation. Compared to the HAADF-STEM image before biasing (Figure 3c), only the upper part of the active material that faces the solid electrolyte becomes distinctly porous with a high density of nanovoids (Figure 4a). The HAADF-STEM image and corresponding EELS elemental maps (Figure 4b,c) show O

https://doi.org/10.1021/acs.nanolett.2c01401
Nano Lett. 2022, 22, 4905−4911

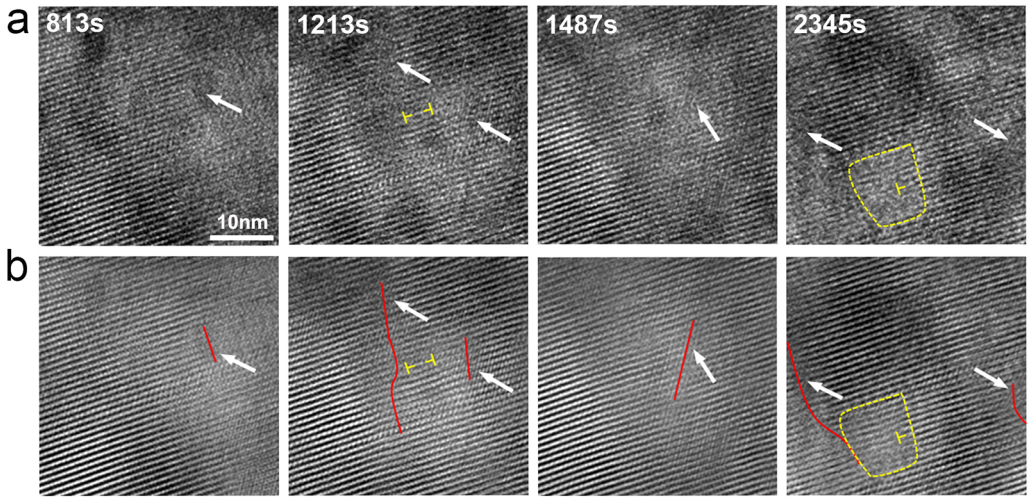

Figure 5. (a,b) Time-lapsed HRTEM images and corresponding filtered images of an enlarged region in LNMO particle in Figure 3 during *in situ* delithiation after image drift correction. The white arrows and red lines indicate the small segment of stacking faults. The yellow symbols indicate dislocations.

and Mn are lacking within the nanovoid, indicating the mass loss. Ni $L_{2,3}$ edge is too weak to notice the local deficiency, which may be due to the short collection time for EELS to protect the sample from the possible beam damage. The 2D relative thickness extracted from low-loss EELS also confirms the mass loss in the nanovoid with the reduced sample thickness. HAADF-STEM images obtained from other LNMO particles (Figure 4d and Figure S7), which were not exposed to the electron beam under biasing, also show a high density of nanovoids which also substantiate that the evolution of a nanovoid is induced by the lithium extraction instead of the electron beam. The degree of porosity development is not consistent among the particles (Figure S7), indicating the degree of lithium removal may be inhomogeneous. This inhomogeneity may result from the kinetic effects, nonuniform contact with electrolytes, and nonuniform electronic/ionic transport. Figure 4e presents the atomic scale HAADF-STEM image focusing on the nanovoid in (b), which demonstrates no obvious cation mixing or phase transformation near the nanovoid. The atomic-resolution HAADF-STEM images are also acquired at the different zone axes ([010] and [110]) (Figure S8), which all show that no aggravating cation mixing occurs around the nanovoid. Similar oxygen vacancy diffusion without phase transition has been recently reported.[42]

To understand how the nanovoid is formed, another *in situ* video (SI Video 3) and corresponding time-lapsed HRTEM images (Figure 5) were trimmed from SI Video 1 after the drift correction, showing the dynamic formation process of a single nanovoid. The region contained one small stacking fault (SF) segment at 813 s, then two SF segments and one pair of dislocations appeared at 1213 s during lithium removal. Later, only one SF segment was left at 1487 s. Finally, a nanovoid formed with two SF segments and one dislocation at 2345 s. These formations, movement, and disappearance of stacking faults and dislocations are observed around the region where the nanovoid is formed, which indicates that the nanovoid formation is strongly related to the defect activities. At a highly delithiated state, oxygen vacancies can be formed to compensate the charge imbalance in lithium-rich cathode materials. They will increase the density of crystalline defects inside the cathode particles, which may accelerate the diffusion of vacancies and/or ions,[29−31] leading the formation and growth of nanovoids without phase transformation (the phase transformation was not observed in our experiment).

It is interesting to note that there are some differences in nanopores and nanovoids. The nanopores are found at the surface of LNMO facing the solid electrolyte with severe cation mixing and structural reconstruction; thus, the spinel-like and rock-salt phase can be easily observed near nanopores. The reduction of Mn and changes in oxygen *K*-edge EELS further demonstrate drastic chemical evolution at the surface of LNMO with LiPON. Therefore, the surface nanopores are closely related to the strain concentration and oxygen loss induced by phase transformations during the spontaneous reaction between the solid electrolyte and cathode.[26] However, the biasing-induced nanovoids are developed inside LNMO with lithium extraction and become bigger by growing and merging with others when more lithium ions are removed. Despite the buildup of nanovoids, the intrinsic layered structure is intact, suggesting that the initial charge process occurs with local mass loss but without phase transformations in the bulk region. This observation may not agree with the widely accepted mechanism of oxygen evolution, which is associated with the phase transformations from the layered structure to the spinel and the rock-salt structures.[21,38,43] The contradiction may have originated from the following factors: (i) our observations focus on the initial lithium extraction occurring at localized areas; (ii) lithium extraction happens unidirectionally here while it takes place more omnidirectionally in a common battery setup, where the active material is immersed in liquid electrolyte; (iii) *in situ* open cell was established in high vacuum TEM chamber. However, Chueh et al. reported the evolution of bulk oxygen vacancy within native layered phase after cycling lithium- manganese-rich cathode material with carbonate-based liquid electrolyte,[42] indicating that the porosity development without cation mixing can be a possible degradation mechanism in lithium- and manganese-rich cathode materials.

In this work, we demonstrate two sources of porous structure in a solid-state battery with the LNMO cathode and LiPON electrolyte. Nanopores are inborn at the surface of LNMO facing with LiPON because of the chemical instability

https://doi.org/10.1021/acs.nanolett.2c01401
Nano Lett. 2022, 22, 4905−4911

between the electrode and electrolyte. Spontaneous chemical reaction also engenders severe cation mixing, phase transition, oxygen loss, and TM reduction. The inherent chemical reactions may be responsible for the interfacial impedance at the cathode surface before applying external electric bias. In the other type of cavity, nanovoids emerged during the charge process or *in situ* lithium-ion extraction. The formation and growth of the nanovoids under *in situ* biasing take place with the formation, movement, and disappearance of defects but without obvious phase evolutions. Our results corroborate the interfacial layer and dynamic evolution of the nanovoids in lithium-, manganese-rich cathode materials with LiPON solid electrolyte, which sheds light on the understanding of performance decay in all-solid-state lithium ion battery.

■ ASSOCIATED CONTENT

Supporting Information

The Supporting Information is available free of charge at https://pubs.acs.org/doi/10.1021/acs.nanolett.2c01401.

Experimental details, HAADF-STEM and *in situ* HRTEM images of LNMO cathode, simulated TEM images, measured *I*−*V* curve during *in situ* biasing, calculated areal portion of nanovoids (PDF)

Video of *in situ* HRTEM observation of a LNMO particle in contact with LiPON during delithiation at a 270 times speed (MP4)

Video of *in situ* HRTEM observation of LNMO particle under the electron dose without biasing at a 270 times speed (MP4)

Video of *in situ* HRTEM observation of a single nanovoid formation at a 25 times speed (MP4)

■ AUTHOR INFORMATION

Corresponding Author

Sooyeon Hwang − *Center for Functional Nanomaterials, Brookhaven National Laboratory, Upton, New York 11973, United States;* orcid.org/0000-0001-5606-6728; Email: soohwang@bnl.gov

Authors

Shuang Li − *Center for Functional Nanomaterials, Brookhaven National Laboratory, Upton, New York 11973, United States;* Present Address: Environmental Molecular Sciences Division, Pacific Northwest National Laboratory, Richland, WA 99352, United States

Yipeng Sun − *Department of Mechanical and Materials Engineering, University of Western Ontario, London, Ontario N6A 6B9, Canada*

Ning Li − *Energy Storage and Distributed Resources Division, Lawrence Berkeley National Laboratory, Berkeley, California 94720, United States*

Wei Tong − *Energy Storage and Distributed Resources Division, Lawrence Berkeley National Laboratory, Berkeley, California 94720, United States;* orcid.org/0000-0002-2878-1297

Xueliang Sun − *Department of Mechanical and Materials Engineering, University of Western Ontario, London, Ontario N6A 6B9, Canada;* orcid.org/0000-0003-0374-1245

Charles T. Black − *Center for Functional Nanomaterials, Brookhaven National Laboratory, Upton, New York 11973, United States*

Complete contact information is available at: https://pubs.acs.org/10.1021/acs.nanolett.2c01401

Author Contributions

S.L. and S.H. designed the experimental plan. S.L. and S.H. performed the TEM experiments and analysis. Y.P.S. and X.L.S. completed the LiPON depositions. N.L. and W.T. provide the LNMO cathode. S.L., C. T. B., and S.H. prepared the manuscripts. All authors contributed to manuscript writing and discussions.

Notes

The authors declare no competing financial interest.

■ ACKNOWLEDGMENTS

This work was supported by the Center for Functional Nanomaterials (CFN), which is a U.S. Department of Energy Office of Science User Facility, at Brookhaven National Laboratory under Contract No. DE-SC0012704. Efforts of the LBNL team are supported by the Assistant Secretary for Energy Efficiency and Renewable Energy, Office of Vehicle Technologies of the U.S. Department of Energy under Contract No. DE-AC02-05CH11231.

■ REFERENCES

(1) Tarascon, J. M.; Armand, M. Issues and challenges facing rechargeable lithium batteries. *Nature* **2001**, *414* (6861), 359−367.

(2) Li, H. Practical Evaluation of Li-Ion Batteries. *Joule* **2019**, *3* (4), 911−914.

(3) Choi, J. W.; Aurbach, D. Promise and reality of post-lithium-ion batteries with high energy densities. *Nat. Rev. Mater.* **2016**, *1* (4), 16013.

(4) Zheng, J.; Myeong, S.; Cho, W.; Yan, P.; Xiao, J.; Wang, C.; Cho, J.; Zhang, J.-G. Li- and Mn-Rich Cathode Materials: Challenges to Commercialization. *Adv. Energy Mater.* **2017**, *7* (6), 1601284.

(5) Wang, J.; He, X.; Paillard, E.; Laszczynski, N.; Li, J.; Passerini, S. Lithium- and Manganese-Rich Oxide Cathode Materials for High-Energy Lithium Ion Batteries. *Adv. Energy Mater.* **2016**, *6* (21), 1600906.

(6) Qiu, B.; Zhang, M.; Xia, Y.; Liu, Z.; Meng, Y. S. Understanding and Controlling Anionic Electrochemical Activity in High-Capacity Oxides for Next Generation Li-Ion Batteries. *Chem. Mater.* **2017**, *29* (3), 908−915.

(7) McCalla, E.; Abakumov, A. M.; Saubanère, M.; Foix, D.; Berg, E. J.; Rousse, G.; Doublet, M.-L.; Gonbeau, D.; Novák, P.; Van Tendeloo, G.; Dominko, R.; Tarascon, J.-M. Visualization of O-O peroxo-like dimers in high-capacity layered oxides for Li-ion batteries. *Science* **2015**, *350* (6267), 1516−1521.

(8) Seo, D.-H.; Lee, J.; Urban, A.; Malik, R.; Kang, S.; Ceder, G. The structural and chemical origin of the oxygen redox activity in layered and cation-disordered Li-excess cathode materials. *Nat. Chem.* **2016**, *8* (7), 692−697.

(9) Ceder, G.; Chiang, Y. M.; Sadoway, D. R.; Aydinol, M. K.; Jang, Y. I.; Huang, B. Identification of cathode materials for lithium batteries guided by first-principles calculations. *Nature* **1998**, *392* (6677), 694−696.

(10) Fang, C.; Li, J.; Zhang, M.; Zhang, Y.; Yang, F.; Lee, J. Z.; Lee, M.-H.; Alvarado, J.; Schroeder, M. A.; Yang, Y.; Lu, B.; Williams, N.; Ceja, M.; Yang, L.; Cai, M.; Gu, J.; Xu, K.; Wang, X.; Meng, Y. S. Quantifying inactive lithium in lithium metal batteries. *Nature* **2019**, *572* (7770), 511−515.

(11) Lin, D.; Liu, Y.; Cui, Y. Reviving the lithium metal anode for high-energy batteries. *Nat. Nanotechnol.* **2017**, *12* (3), 194−206.

(12) Yu, X.; Bates, J. B.; Jellison, G. E.; Hart, F. X. A Stable Thin-Film Lithium Electrolyte: Lithium Phosphorus Oxynitride. *J. Electrochem. Soc.* **1997**, *144* (2), 524−532.

(13) Zhu, Y.; He, X.; Mo, Y. First principles study on electrochemical and chemical stability of solid electrolyte−electrode

interfaces in all-solid-state Li-ion batteries. *J. Mater. Chem. A* **2016**, *4* (9), 3253−3266.
(14) Hood, Z. D.; Chen, X.; Sacci, R. L.; Liu, X.; Veith, G. M.; Mo, Y.; Niu, J.; Dudney, N. J.; Chi, M. Elucidating Interfacial Stability between Lithium Metal Anode and Li Phosphorus Oxynitride via In Situ Electron Microscopy. *Nano Lett.* **2021**, *21* (1), 151−157.
(15) Li, J.; Ma, C.; Chi, M.; Liang, C.; Dudney, N. J. Solid Electrolyte: the Key for High-Voltage Lithium Batteries. *Adv. Energy Mater.* **2015**, *5* (4), 1401408.
(16) Yang, P.; Zheng, J.; Kuppan, S.; Li, Q.; Lv, D.; Xiao, J.; Chen, G.; Zhang, J.-G.; Wang, C.-M. Phosphorus Enrichment as a New Composition in the Solid Electrolyte Interphase of High-Voltage Cathodes and Its Effects on Battery Cycling. *Chem. Mater.* **2015**, *27* (21), 7447−7451.
(17) Xu, K. Electrolytes and Interphases in Li-Ion Batteries and Beyond. *Chem. Rev.* **2014**, *114* (23), 11503−11618.
(18) Xu, B.; Fell, C. R.; Chi, M.; Meng, Y. S. Identifying surface structural changes in layered Li-excess nickel manganeseoxides in high voltage lithium ion batteries: A joint experimental and theoretical study. *Energy Environ. Sci.* **2011**, *4* (6), 2223.
(19) Boulineau, A.; Simonin, L.; Colin, J.-F.; Canévet, E.; Daniel, L.; Patoux, S. Evolutions of $Li_{1.2}Mn_{0.61}Ni_{0.18}Mg_{0.01}O_2$ during the Initial Charge/Discharge Cycle Studied by Advanced Electron Microscopy. *Chem. Mater.* **2012**, *24* (18), 3558−3566.
(20) Mohanty, D.; Sefat, A. S.; Kalnaus, S.; Li, J.; Meisner, R. A.; Payzant, E. A.; Abraham, D. P.; Wood, D. L.; Daniel, C. Investigating phase transformation in the $Li_{1.2}Co_{0.1}Mn_{0.55}Ni_{0.15}O_2$ lithium-ion battery cathode during high-voltage hold (4.5 V) via magnetic, X-ray diffraction and electron microscopy studies. *J. Mater. Chem. A* **2013**, *1* (20), 6249.
(21) Zheng, J.; Xu, P.; Gu, M.; Xiao, J.; Browning, N. D.; Yan, P.; Wang, C.; Zhang, J.-G. Structural and Chemical Evolution of Li- and Mn-Rich Layered Cathode Material. *Chem. Mater.* **2015**, *27* (4), 1381−1390.
(22) Zheng, J.; Gu, M.; Xiao, J.; Zuo, P.; Wang, C.; Zhang, J.-G. Corrosion/Fragmentation of Layered Composite Cathode and Related Capacity/Voltage Fading during Cycling Process. *Nano Lett.* **2013**, *13* (8), 3824−3830.
(23) Yan, P.; Zheng, J.; Tang, Z.-K.; Devaraj, A.; Chen, G.; Amine, K.; Zhang, J.-G.; Liu, L.-M.; Wang, C. Injection of oxygen vacancies in the bulk lattice of layered cathodes. *Nat. Nanotechnol.* **2019**, *14* (6), 602−608.
(24) Luntz, A. C.; Voss, J.; Reuter, K. Interfacial Challenges in Solid-State Li Ion Batteries. *J. Phys. Chem. Lett.* **2015**, *6* (22), 4599−4604.
(25) Yada, C.; Ohmori, A.; Ide, K.; Yamasaki, H.; Kato, T.; Saito, T.; Sagane, F.; Iriyama, Y. Dielectric Modification of 5V-Class Cathodes for High-Voltage All-Solid-State Lithium Batteries. *Adv. Energy Mater.* **2014**, *4* (9), 1301416.
(26) Wang, Z.; Santhanagopalan, D.; Zhang, W.; Wang, F.; Xin, H. L.; He, K.; Li, J.; Dudney, N.; Meng, Y. S. In Situ STEM-EELS Observation of Nanoscale Interfacial Phenomena in All-Solid-State Batteries. *Nano Lett.* **2016**, *16* (6), 3760−3767.
(27) Gong, Y.; Zhang, J.; Jiang, L.; Shi, J. A.; Zhang, Q.; Yang, Z.; Zou, D.; Wang, J.; Yu, X.; Xiao, R.; Hu, Y. S.; Gu, L.; Li, H.; Chen, L. In Situ Atomic-Scale Observation of Electrochemical Delithiation Induced Structure Evolution of $LiCoO_2$ Cathode in a Working All-Solid-State Battery. *J. Am. Chem. Soc.* **2017**, *139* (12), 4274−4277.
(28) Ong, P. V.; Yang, Z.; Sushko, P. V.; Du, Y. Formation, Structural Variety, and Impact of Antiphase Boundaries on Li Diffusion in $LiCoO_2$ Thin-Film Cathodes. *J. Phys. Chem. Lett.* **2018**, *9* (18), 5515−5520.
(29) Yang, Z.; Ong, P. V.; He, Y.; Wang, L.; Bowden, M. E.; Xu, W.; Droubay, T. C.; Wang, C.; Sushko, P. V.; Du, Y. Direct Visualization of Li Dendrite Effect on $LiCoO_2$ Cathode by In Situ TEM. *Small* **2018**, *14* (52), 1803108.
(30) Li, Q.; Yao, Z.; Lee, E.; Xu, Y.; Thackeray, M. M.; Wolverton, C.; Dravid, V. P.; Wu, J. Dynamic imaging of crystalline defects in lithium-manganese oxide electrodes during electrochemical activation to high voltage. *Nat. Commun.* **2019**, *10* (1), 1692.
(31) Li, S.; Yao, Z.; Zheng, J.; Fu, M.; Cen, J.; Hwang, S.; Jin, H.; Orlov, A.; Gu, L.; Wang, S.; Chen, Z.; Su, D. Direct Observation of Defect-Aided Structural Evolution in a Nickel-Rich Layered Cathode. *Angew. Chem., Int. Ed.* **2020**, *59* (49), 22092−22099.
(32) Lei, C. H.; Wen, J. G.; Sardela, M.; Bareño, J.; Petrov, I.; Kang, S. H.; Abraham, D. P. Structural study of Li_2MnO_3 by electron microscopy. *J. Mater. Sci.* **2009**, *44* (20), 5579−5587.
(33) Meng, Y. S.; Ceder, G.; Grey, C. P.; Yoon, W. S.; Jiang, M.; Bréger, J.; Shao-Horn, Y. Cation Ordering in Layered O3 $Li[Ni_xLi_{1/3-2x/3}Mn_{2/3-x/3}]O_2$ ($0 \le x \le 1/2$) Compounds. *Chem. Mater.* **2005**, *17* (9), 2386−2394.
(34) Shukla, A. K.; Ramasse, Q. M.; Ophus, C.; Duncan, H.; Hage, F.; Chen, G. Unravelling structural ambiguities in lithium- and manganese-rich transition metal oxides. *Nat. Commun.* **2015**, *6*, 8711.
(35) Sugawara, Y.; Taminato, S.; Hirayama, T.; Hirayama, M.; Kanno, R.; Ukyo, Y.; Ikuhara, Y. Interfacial Atomic Structures of Single-Phase Li_2MnO_3 Thin Film with Superior Initial Charge-Discharge Behavior. *J. Electrochem. Soc.* **2018**, *165* (2), A55−A60.
(36) Aydinol, M. K.; Kohan, A. F.; Ceder, G.; Cho, K.; Joannopoulos, J. Ab initio study of lithium intercalation in metal oxides and metal dichalcogenides. *Phys. Rev. B* **1997**, *56* (3), 1354−1365.
(37) Liu, H.; Bugnet, M.; Tessaro, M. Z.; Harris, K. J.; Dunham, M. J.; Jiang, M.; Goward, G. R.; Botton, G. A. Spatially resolved surface valence gradient and structural transformation of lithium transition metal oxides in lithium-ion batteries. *Phys. Chem. Chem. Phys.* **2016**, *18* (42), 29064−29075.
(38) Zheng, J.; Gu, M.; Xiao, J.; Polzin, B. J.; Yan, P.; Chen, X.; Wang, C.; Zhang, J.-G. Functioning Mechanism of AlF_3 Coating on the Li- and Mn-Rich Cathode Materials. *Chem. Mater.* **2014**, *26* (22), 6320−6327.
(39) Gu, M.; Genc, A.; Belharouak, I.; Wang, D.; Amine, K.; Thevuthasan, S.; Baer, D. R.; Zhang, J.-G.; Browning, N. D.; Liu, J.; Wang, C. Nanoscale Phase Separation, Cation Ordering, and Surface Chemistry in Pristine $Li_{1.2}Ni_{0.2}Mn_{0.6}O_2$ for Li-Ion Batteries. *Chem. Mater.* **2013**, *25* (11), 2319−2326.
(40) Wang, Z.; Lee, J. Z.; Xin, H. L.; Han, L.; Grillon, N.; Guy-Bouyssou, D.; Bouyssou, E.; Proust, M.; Meng, Y. S. Effects of cathode electrolyte interfacial (CEI) layer on long term cycling of all-solid-state thin-film batteries. *J. Power Sources* **2016**, *324*, 342−348.
(41) Lee, J.; Urban, A.; Li, X.; Su, D.; Hautier, G.; Ceder, G. Unlocking the Potential of Cation-Disordered Oxides for Rechargeable Lithium Batteries. *Science* **2014**, *343* (6170), 519−522.
(42) Csernica, P. M.; Kalirai, S. S.; Gent, W. E.; Lim, K.; Yu, Y.-S.; Liu, Y.; Ahn, S.-J.; Kaeli, E.; Xu, X.; Stone, K. H.; Marshall, A. F.; Sinclair, R.; Shapiro, D. A.; Toney, M. F.; Chueh, W. C. Persistent and partially mobile oxygen vacancies in Li-rich layered oxide. *Nat. Energy* **2021**, *6* (6), 642−652.
(43) Nam, K.-W.; Bak, S.-M.; Hu, E.; Yu, X.; Zhou, Y.; Wang, X.; Wu, L.; Zhu, Y.; Chung, K.-Y.; Yang, X.-Q. Combining In Situ Synchrotron X-Ray Diffraction and Absorption Techniques with Transmission Electron Microscopy to Study the Origin of Thermal Instability in Overcharged Cathode Materials for Lithium-Ion Batteries. *Adv. Funct. Mater.* **2013**, *23* (8), 1047−1063.

https://doi.org/10.1021/acs.nanolett.2c01401
Nano Lett. 2022, 22, 4905−4911